Electronic Supplementary Material (ESI) for Metallomics.

Supplementary Information

to

Impact of naturally occurring serine/cysteine variations on the structure and function of *Pseudomonas* metallothioneins

Jelena Habjanič, Serge Chesnov, Oliver Zerbe, Eva Freisinger

Table of Content

```
                        GGA TCC GAG AAC CTT TAC TTC CAA
                         BamHI   E   N   L   Y   F   Q
Optimized DNA sequence  AAC GAT CAG CGC TGC GCG TGC ACC CAT TGC AGC TGC ACC GTG GAT GCG AAC
DNA sequence of PpKT MT AAC GAT CAA CGC TGC GCG TGT ACG CAC TGT TCC TGC ACT GTG GAT GCC AAT
Translation              N   D   Q   R   C   A   C   T   H   C   S   C   T   V   D   A   N
                        GCG CTG CAG CGC GAT GGC AAA GCG TAT TGC TGC GAA GCG TGC GCG AGC GGC
                        GCC TTG CAG CGC GAC GGC AAG GCC TAT TGC TGC GAG GCC TGC GCC AGC GGC
                         A   L   Q   R   D   G   K   A   Y   C   C   E   A   C   A   S   G
                        CAT CGC AAA GGC GAA CCG TGC CGC ATG CAG GAT TGC CAT TGC GGC GAA AAA
                        CAC CGC AAG GGT GAG CCC TGC CGG ATG CAG GAC TGC CAT TGT GGT GAG AAG
                         H   R   K   G   E   P   C   R   M   Q   D   C   H   C   G   E   K
                        CCG GGC GAA AGC GCG GTG GAT AAC GCG CTG GAT GAA ACC TTT CCG GCG AGC
                        CCG GGC GAG AGC GCG GTG GAC AAT GCG TTG GAT GAA ACC TTC CCA GCG AGT
                         P   G   E   S   A   V   D   N   A   L   D   E   T   F   P   A   S
                        GAT CCG ATT AGC CCG TGA
                        GAT CCG ATC TCG CCC
                         D   P   I   S   P  stop
                        CCC GGG
                        XmaI
```

Figure S1. Codon usage for PpKT MT and gene optimization for expression in *E. coli*.

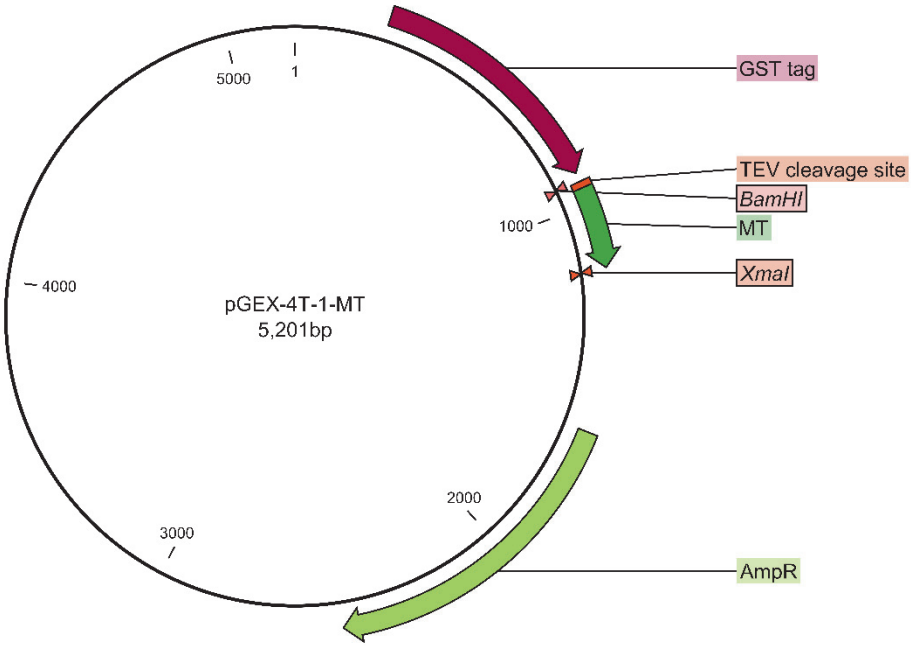

Figure S2. Plasmid map of pGEX-4T-1-MT expression vector.

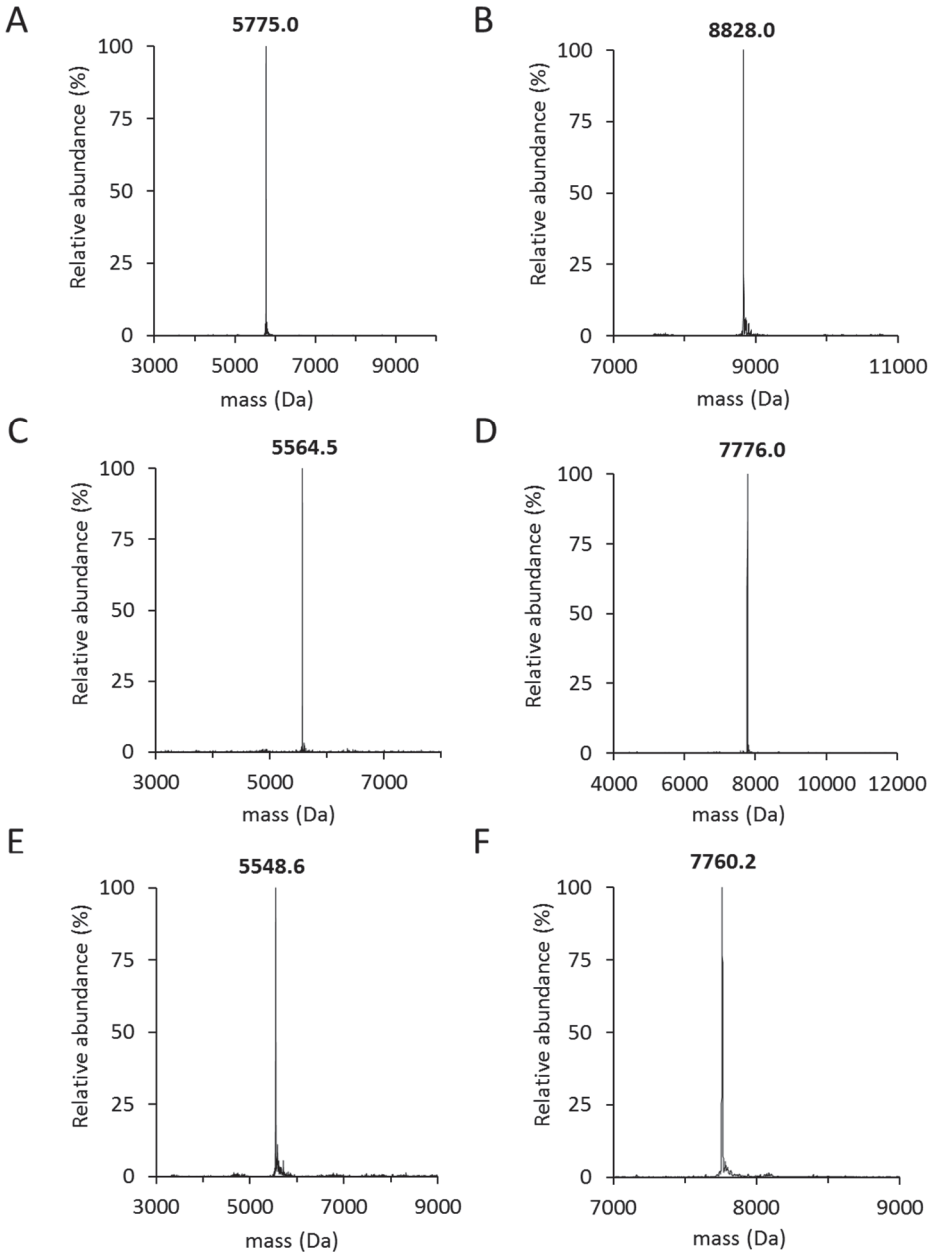

Figure S3. Deconvoluted ESI(+) mass spectra of the apo forms of A) S29C-sh_PflQ2 MT (M_{calc} 5775.34 Da), B) S29C-PflQ2 MT (M_{calc} 8828.62 Da), C) sh_PpKT MT (M_{calc} 5565.21 Da), D) PpKT MT (M_{calc} 7776.53 Da), E) C28S-sh_PpKT MT (M_{calc} 5549.15 Da), and F) C28S-PpKT MT (M_{calc} 7760.47 Da).

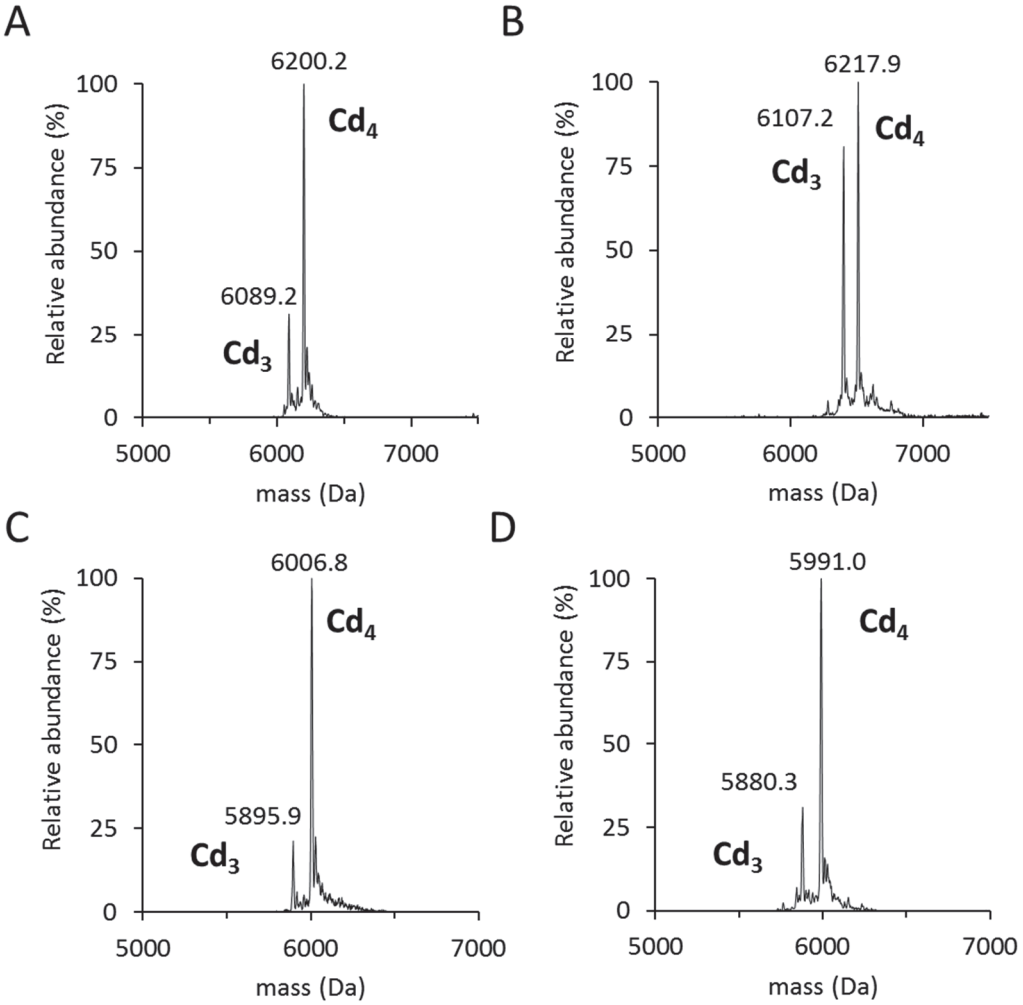

Figure S4. Deconvoluted ESI(+) mass spectra for Cd^{II} species of A) sh_PflQ2 MT (M_{calc} 6199.92 Da (Cd_4),[1] 6087.51 Da (Cd_3)), B) S29C-sh_PflQ2 MT (M_{calc} 6216.58 Da (Cd_4), 6104.17 Da (Cd_3)), C) sh_PpKT MT (M_{calc} 6008.91 Da (Cd_4), 5897.91 Da (Cd_3)), and D) C28S-sh_PpKT MT (M_{calc} 5993.15 (Cd_4), 5882.15 (Cd_3)).

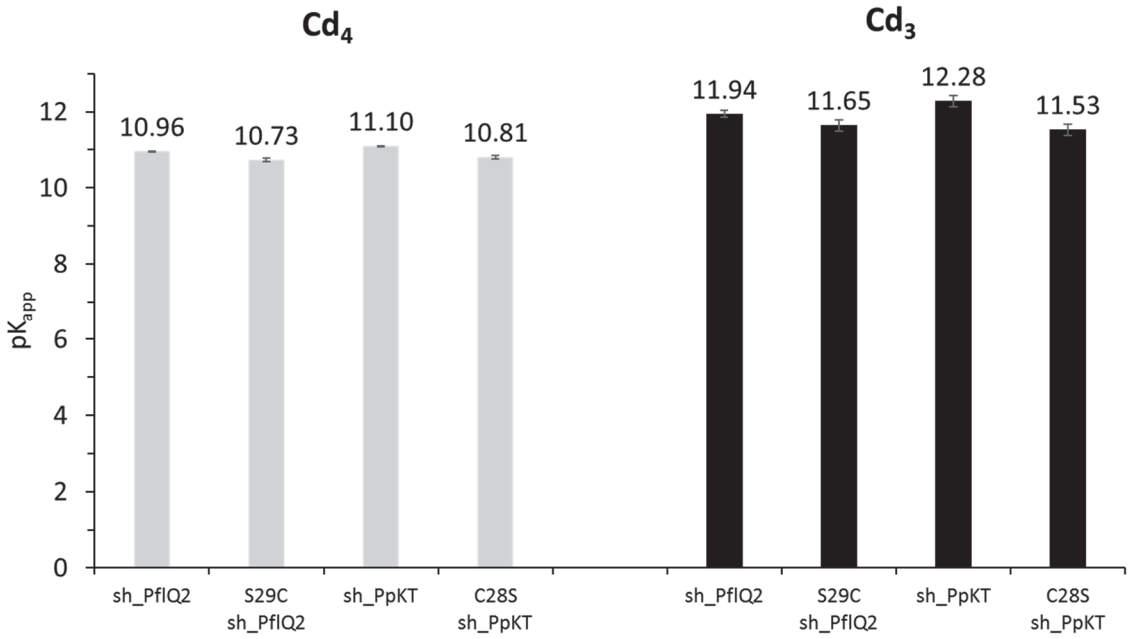

Figure S5. Log values for average apparent binding constants, pK_{app}, (I=321 mM) for the Cd_4 and the Cd_3 species of sh_PflQ2 MT, S29C-sh_PflQ2 MT, sh_PpKT MT, and C28S-sh_PpKT MT.

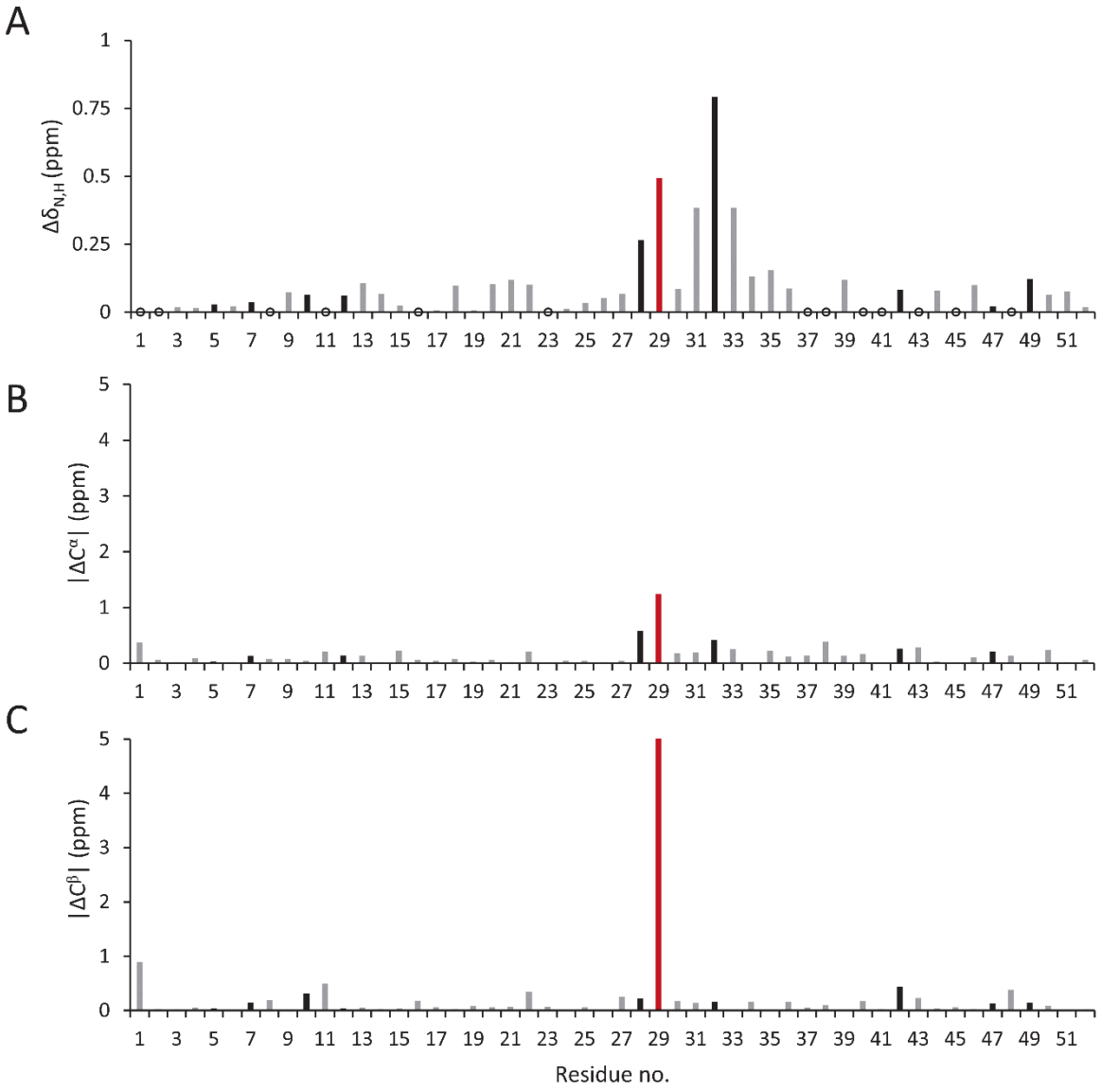

Figure S6. Analysis of chemical shift differences between Cd_4 species of sh_PflQ2 MT and its S29C mutant for A) backbone, B) C^{α}, and C) C^{β}. Cys residues are represented with black bars, while red bars represent the position of Ser/Cys variation. Values that could not be determined are indicated by ○.

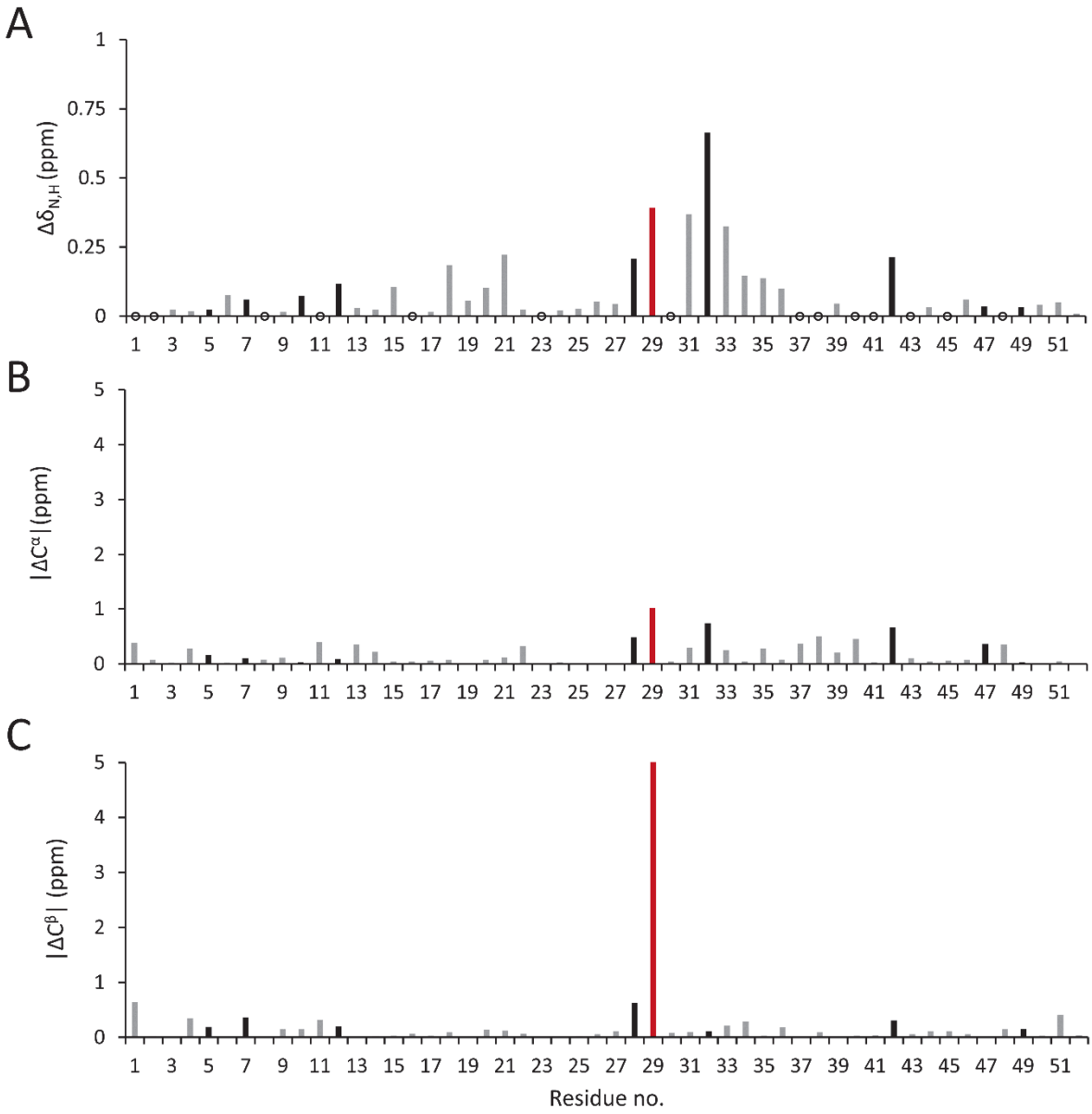

Figure S7. Analysis of chemical shift differences between Cd_3 species of sh_PflQ2 MT and its S29C mutant for A) backbone, B) C^{α}, and C) C^{β}. Cys residues are represented with black bars, while red bars represent the position of Ser/Cys variation. Values that could not be determined are indicated by ○.

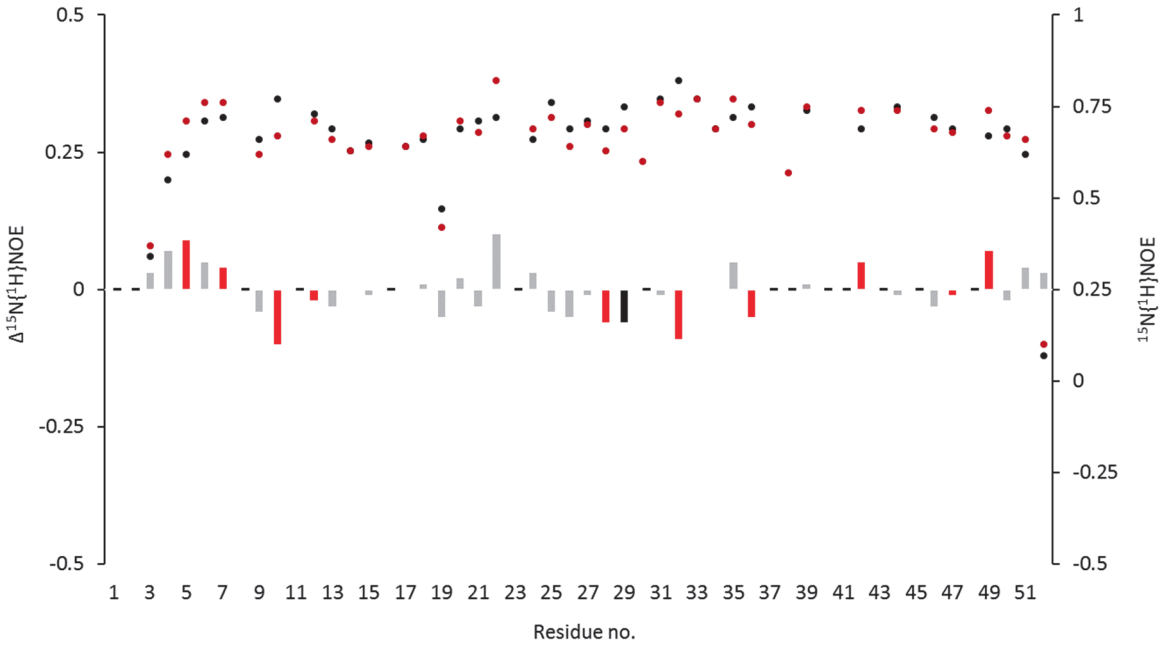

Figure S8. Comparison of $^{15}N\{^{1}H\}$-NOE values for Cd_4 species of sh_PflQ2 MT (black circles) and its S29C mutant (red circles). Difference between the two values are represented by grey columns with Cys residues highlighted in red and residue position 29 in black.

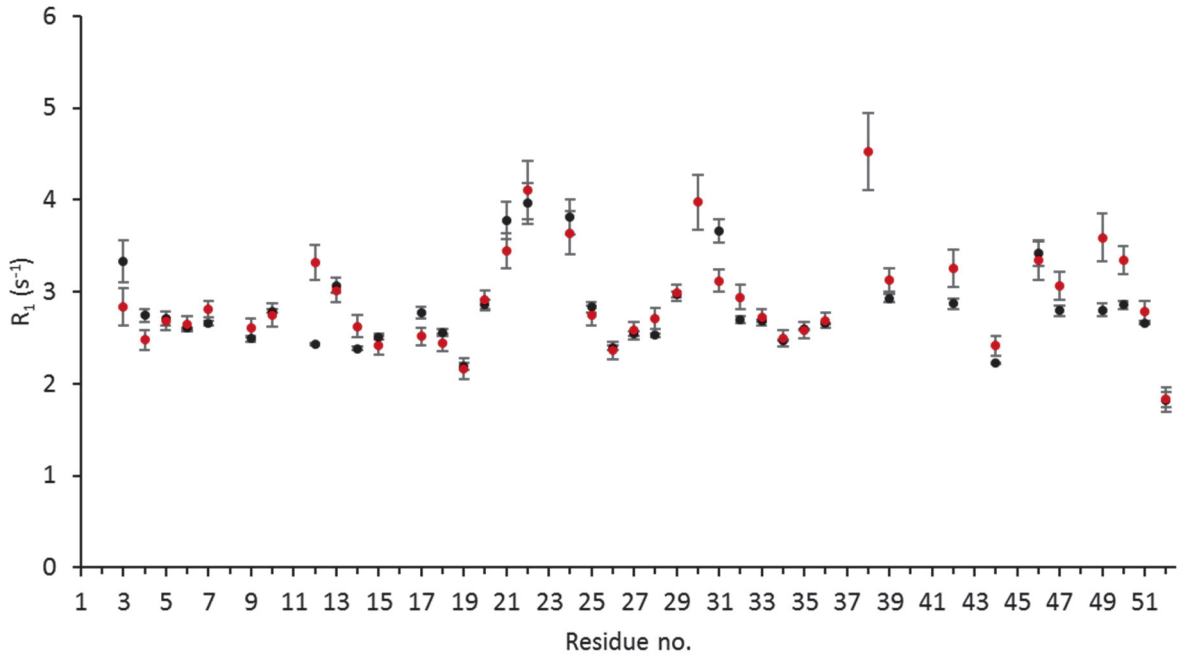

Figure S9. Longitudinal R_1 relaxation rates for Cd_4 species of sh_PflQ2 MT (black circles) and its S29C mutant (red circles).

.

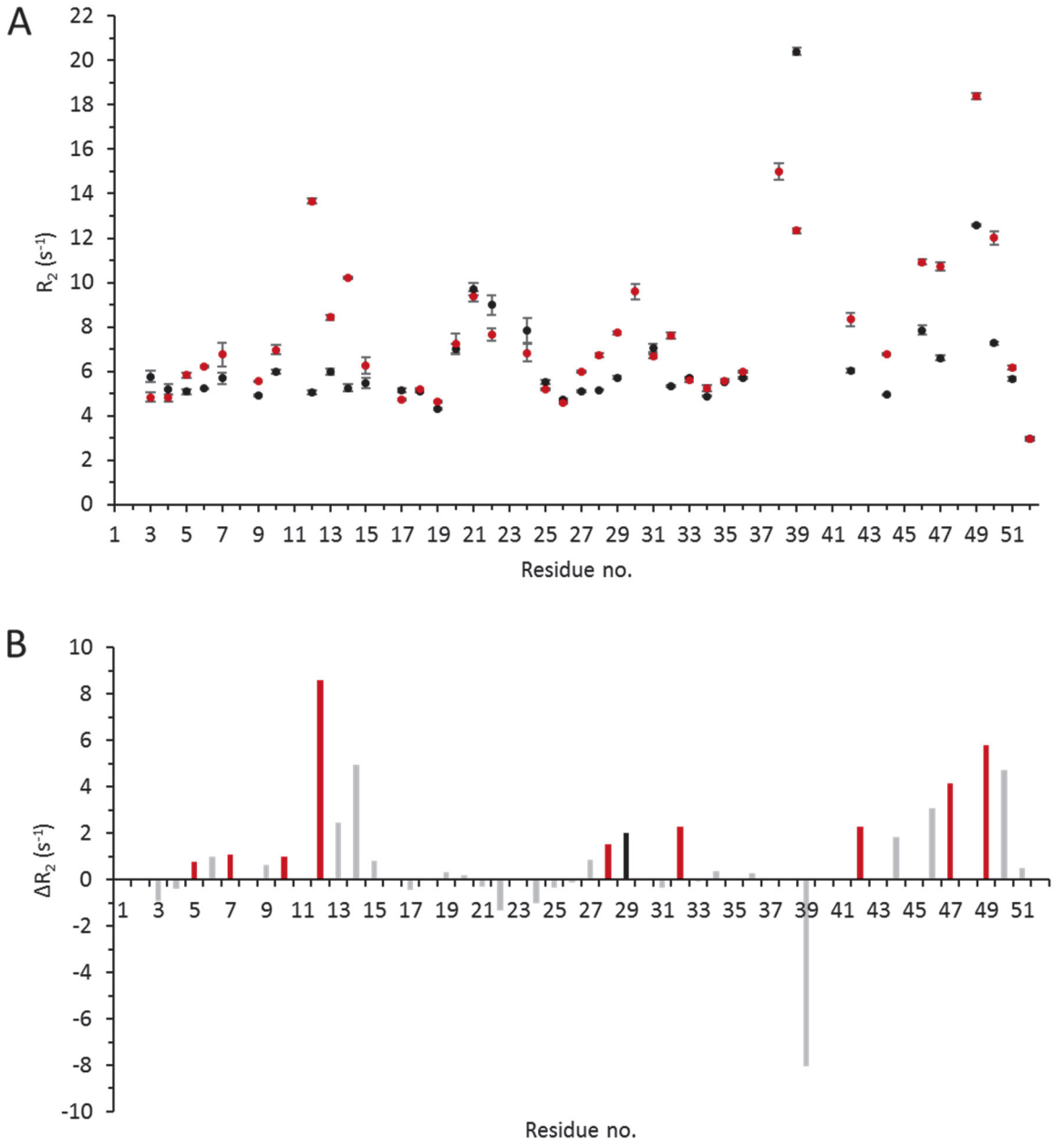

Figure S10. A) Transverse R_2 relaxation rates of Cd_4 species of sh_PflQ2 MT (black circles) and its S29C mutant (red circles). B) Difference between the R_2 values (residue 29 highlighted in black, Cys residue in red).

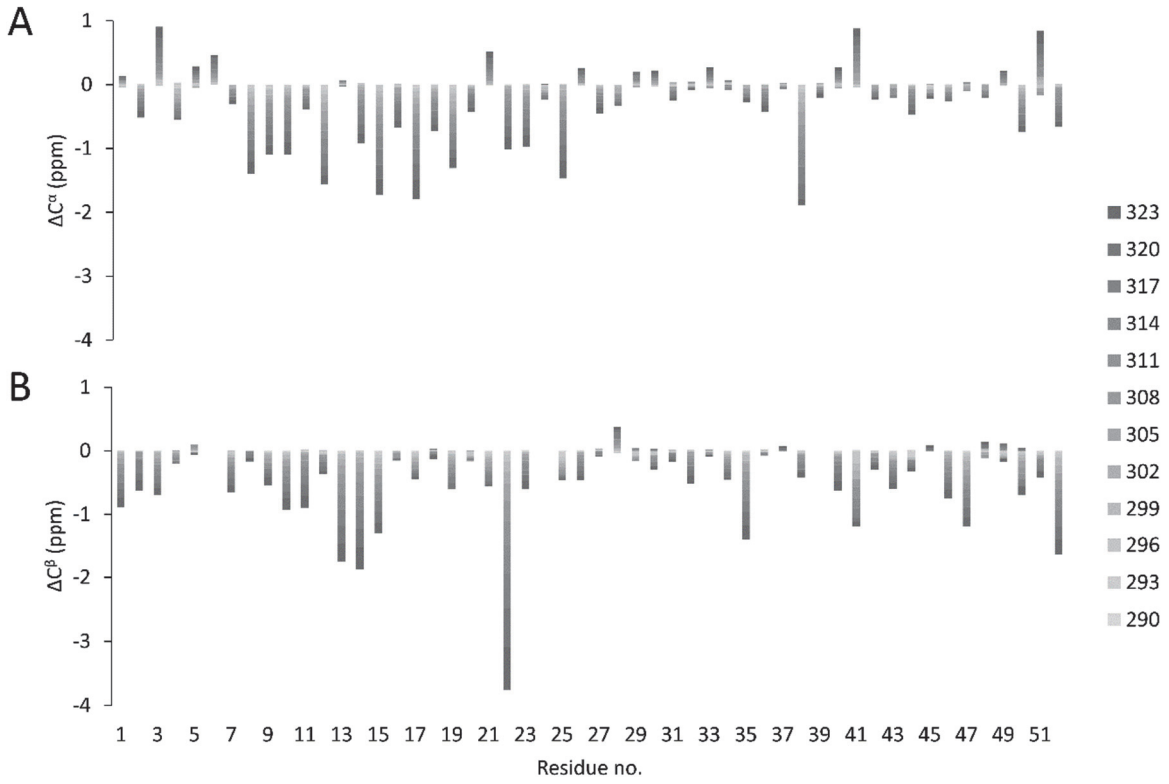

Figure S11. NMR melting studies. The difference in chemical shift changes of A) C^{α} and B) C^{β} between Cd_4 species of sh_PflQ2 MT and its S29C mutant upon temperature increase from 290 K to 323 K.

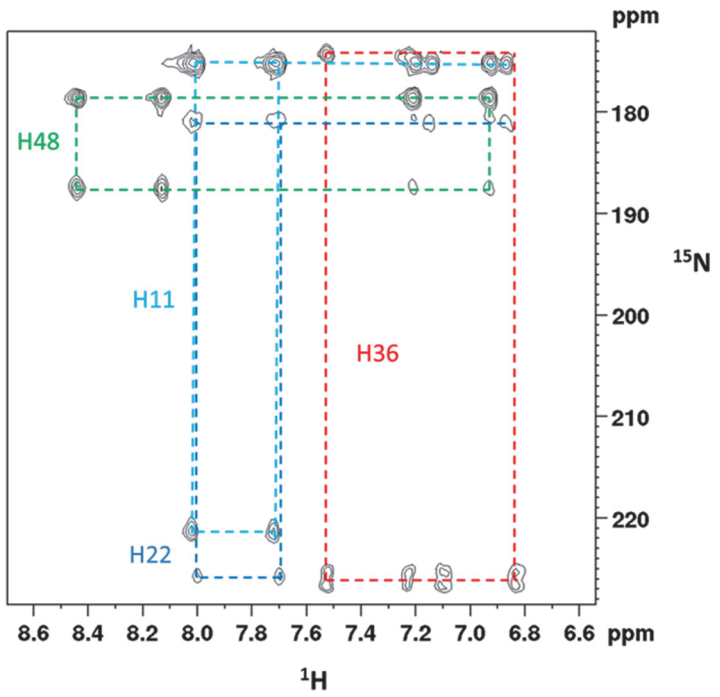

Figure S12 Long-range [^{15}N, ^{1}H]-HSQC spectrum of Cd_4S29C-sh_PflQ2 MT at 300 K, J (^{15}N, ^{1}H) = 30 Hz.

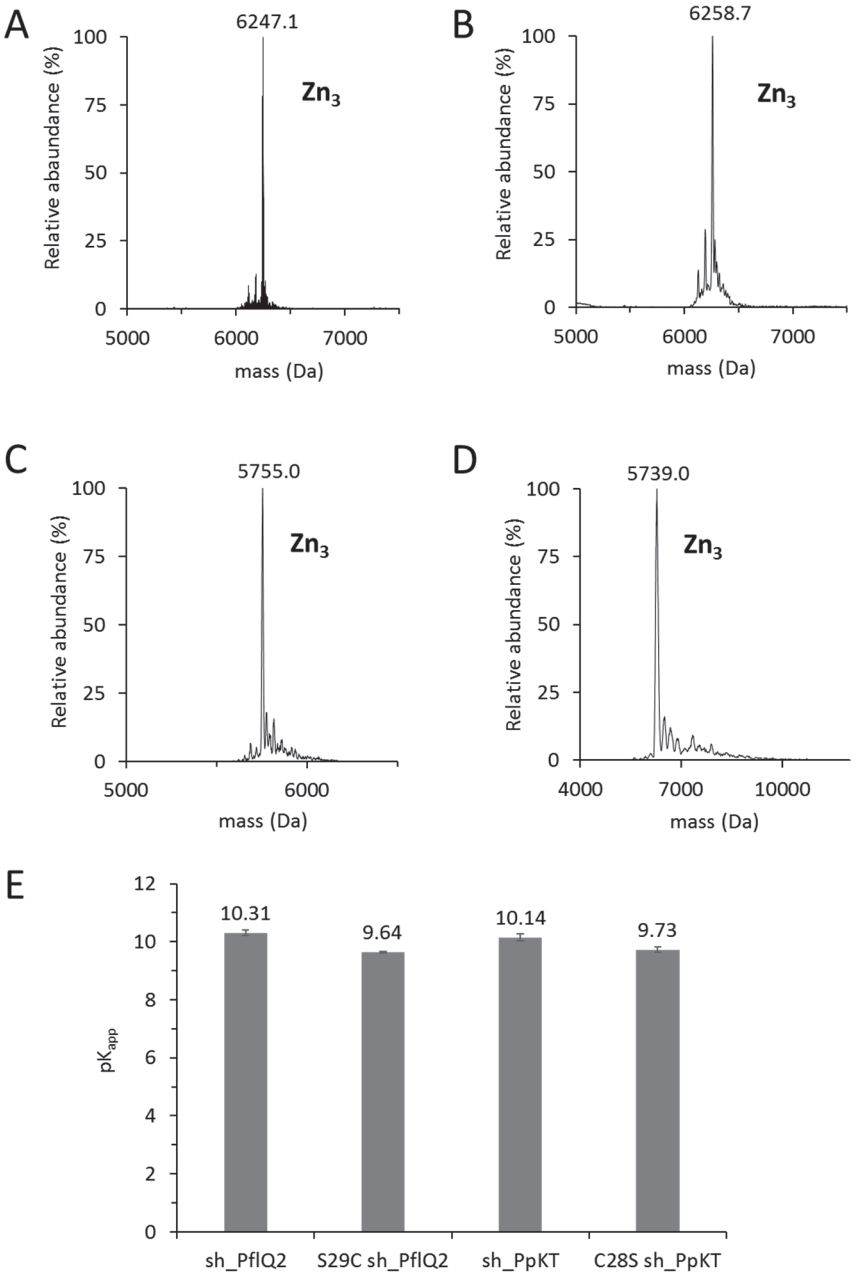

Figure S13. Deconvoluted ESI(+) mass spectra of Zn_3 species of A) sh_PflQ2 MT (M_{calc} 6250.16; ^{13}C, ^{15}N labelled protein) B) S29C-sh_PflQ2 MT (M_{calc} 6264.94; ^{13}C, ^{15}N labelled protein) C) sh_PpKT MT (M_{calc} 5761.35) D) C28S sh-PpKT MT (M_{calc} 5745.38) E) Log values for average apparent binding constants pK_{app} (I=321 mM) for the Zn_3 species of sh_PflQ2 MT and sh_PpKT and their S29C and C28S mutants respectively.

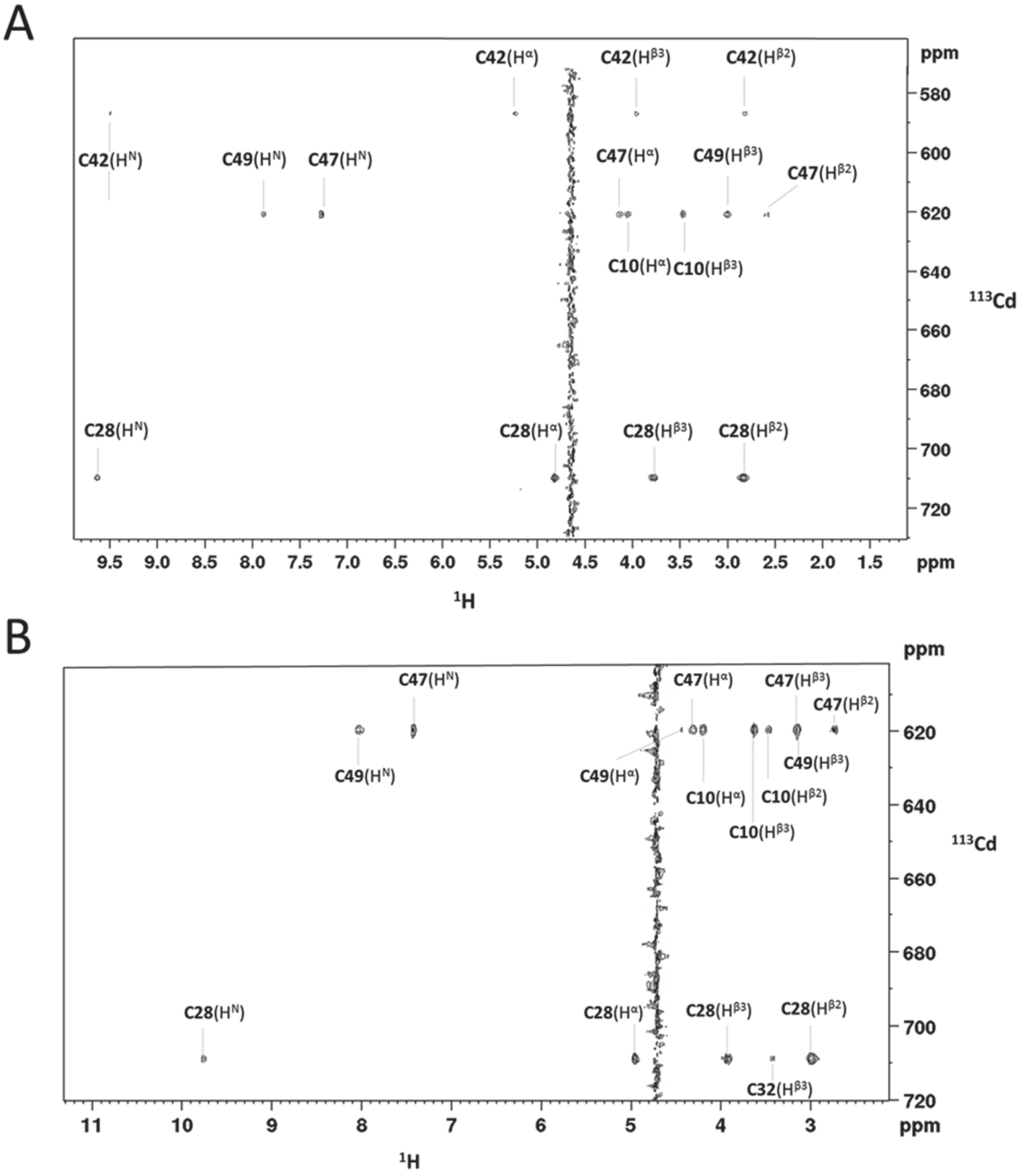

Figure S14. [^{113}Cd,^{1}H]-HSQC-TOCSY spectra of Cd_4S29C-sh_PflQ2 MT at A) 310 K and B) 320 K, J (^{113}Cd, ^{1}H) = 40 Hz.

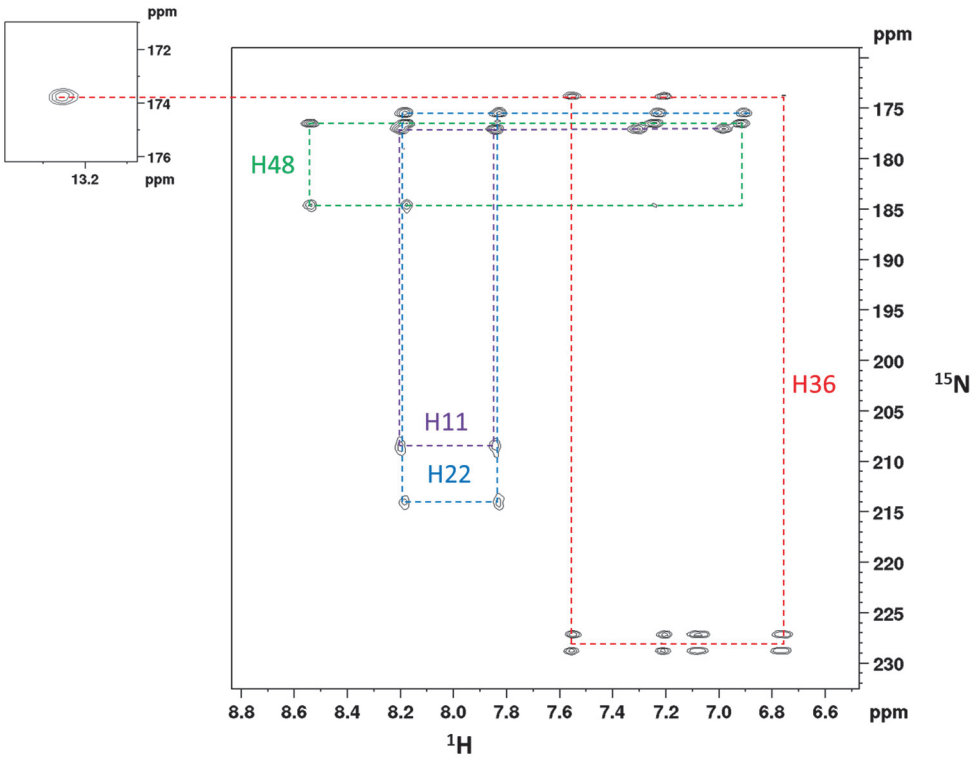

Figure S15. Long-range [^{15}N,^{1}H] spectrum of Cd_3S29C-sh_PflQ2 at 300 K, J (^{15}N, ^{1}H) = 22.25 Hz.

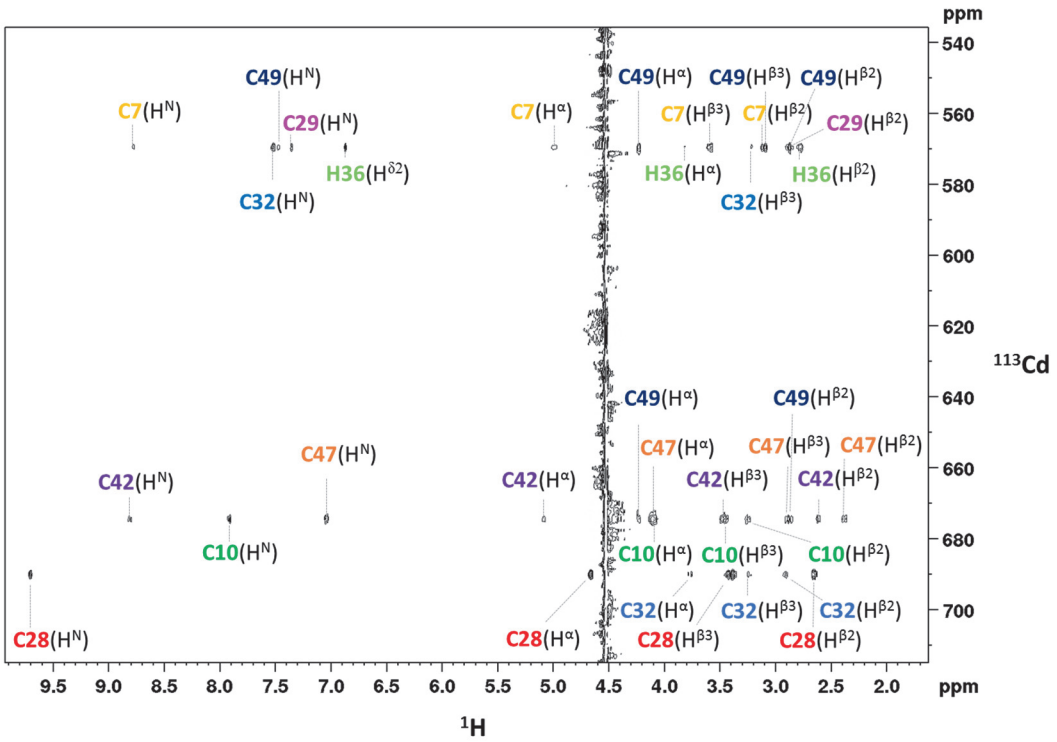

Figure S16. [^{113}Cd,^{1}H]-HSQC-TOCSY spectrum of Cd_3S29C-sh_PflQ2 MT at 320 K, J (^{113}Cd, ^{1}H) = 35 Hz.

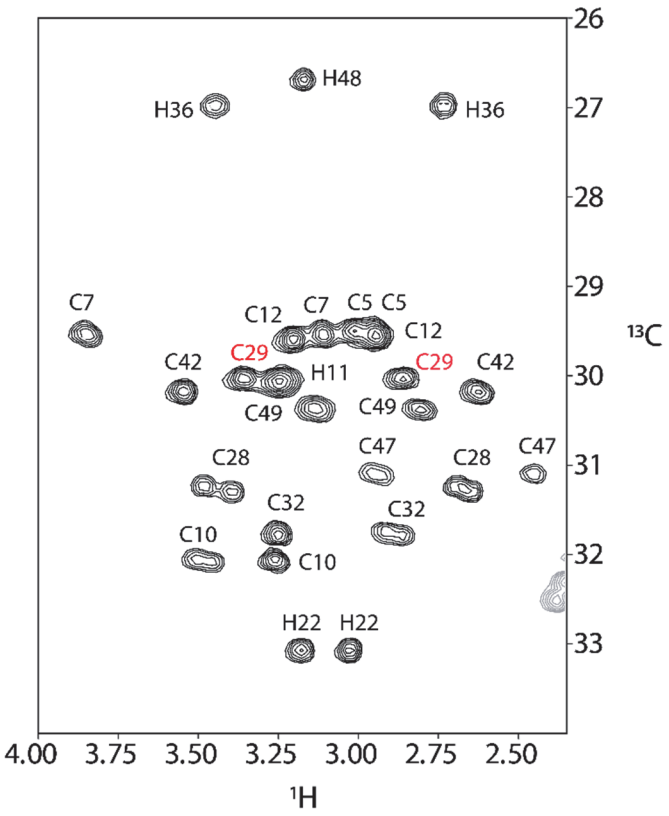

Figure S17. [^{13}C,^{1}H]-HSQC spectrum of Cd_3S29C-sh_PflQ2 MT showing H^{β}-C^{β} correlations of Cys and His residues.

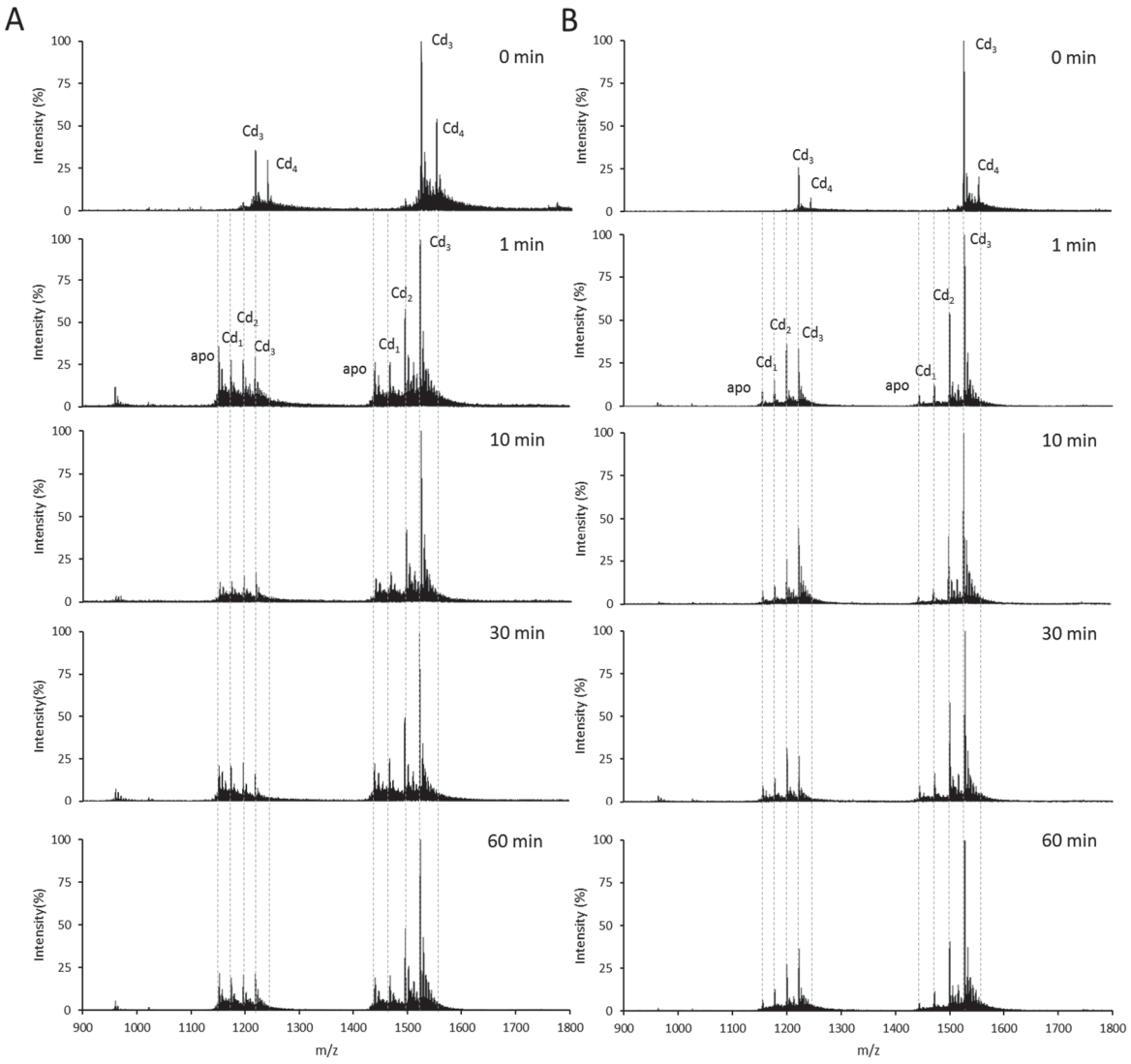

Figure S18. ESI(+) mass spectra of different Cd_4 species and four equivalents of EDTA (⇒ Cd : EDTA = 1:1) taken at the specified time points: A) sh_PflQ2 MT, and B) S29C-sh_PflQ2 MT.

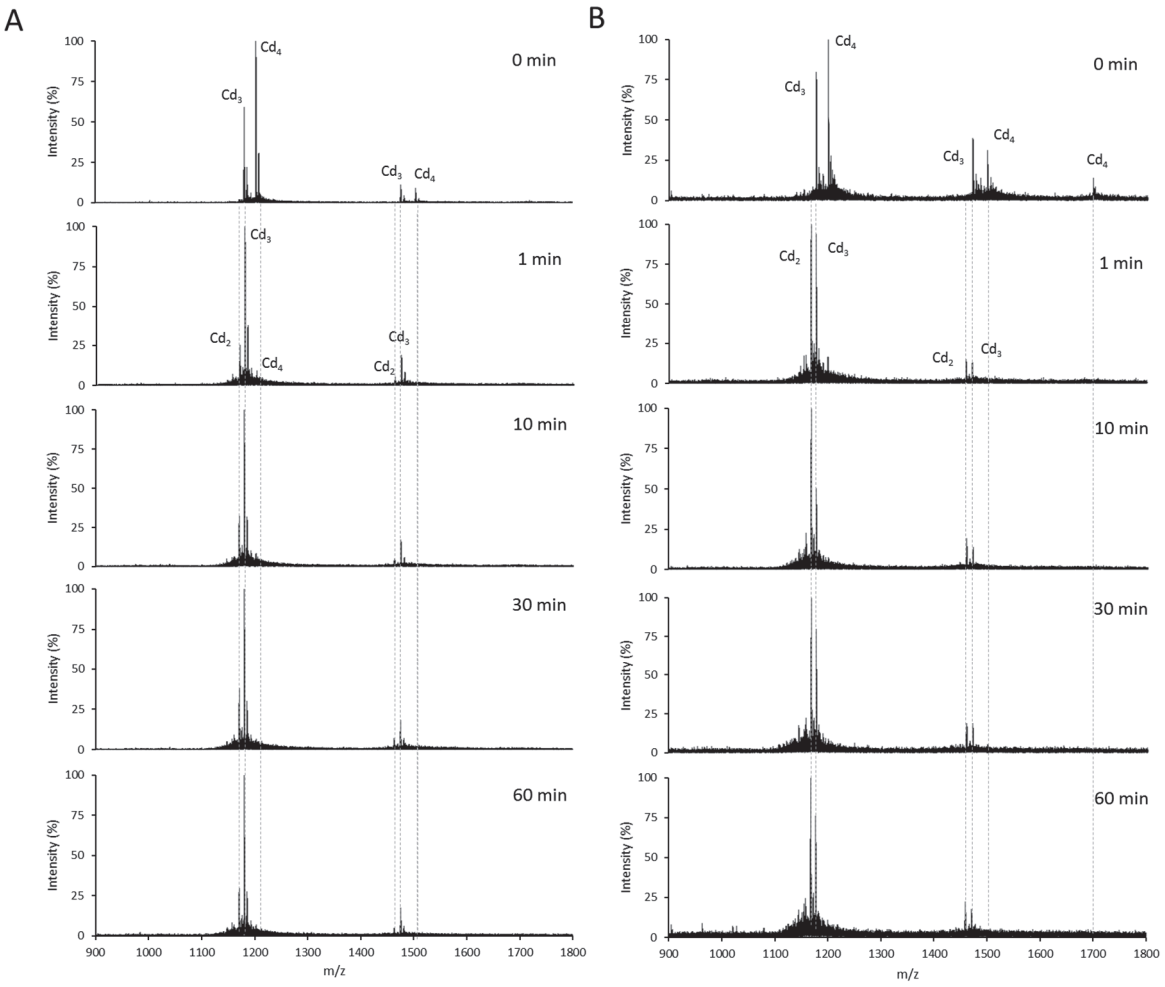

Figure S19. ESI(+) mass spectra of different Cd_4 species and four equivalents of EDTA ($\Rightarrow$ Cd : EDTA = 1:1) taken at the specified time points: A) sh_PpKT MT, and B) C28S-sh_PpKT MT.

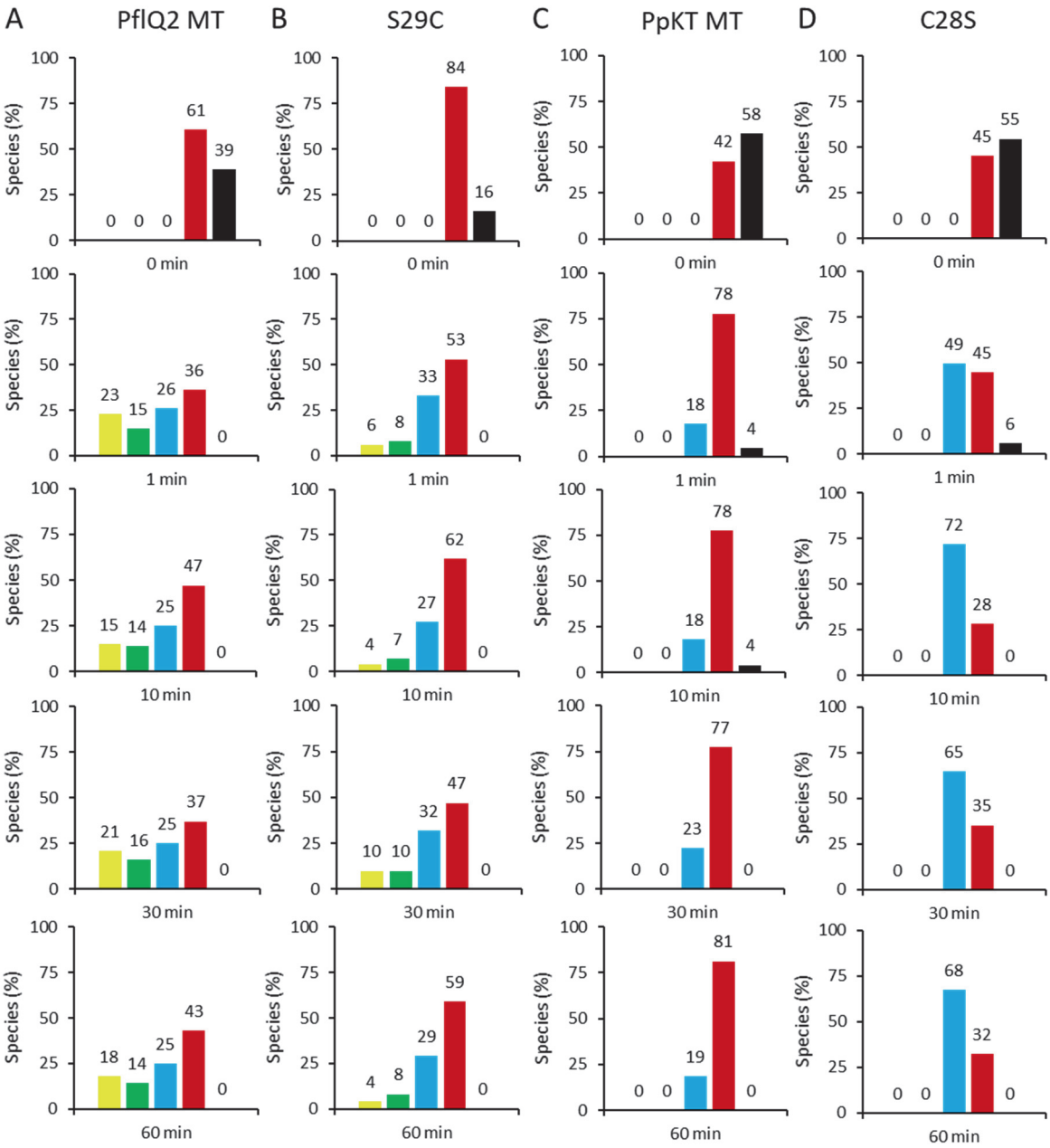

Figure S20. Cadmium transfer from MT to EDTA. 10 µM solutions of the respective MT, prepared by addition of four equiv. of Cd^{II} to the apo protein, were incubated with 40 µM EDTA.The figure shows the percentage of individual species detected by ESI-MS before (0 min) and 1, 10, 30, and 60 min after the addition of EDTA. Apo-forms are depicted by yellow bars, Cd_1 species by green, Cd_2 by blue, Cd_3 by red, and Cd_4 by black bars. A) Cd_4PflQ2 MT, B) Cd_4S29C-PflQ2 MT, C) Cd_4PpKT, D) Cd_4C28S-PpKT MT.

Table S1. List of primers used for the construction of coding sequences.

Q88HU1_F1_fwd	GCG AAT TGG ATC CGA GAA CCT TTA CTT CCA AAA CGA TCA GCG CTG CGC GTG CAC CCA TTG C
Q88HU1_R2_rev	GCT GCA GCG CGT TCG CAT CCA CGG TGC AGC TGC AAT GGG TGC ACG C
Q88HU1_R3_rev	CGC GCA CGC TTC GCA GCA ATA CGC TTT GCC ATC GCG CTG CAG CGC GTT C
Q88HU1_R4_rev	GGC ACG GTT CGC CTT TGC GAT GGC CGC TCG CGC ACG CTT CG
Q88HU1_R5_rev	GCC CGG TTT TTC GCC GCA ATG GCA ATC CTG CAT GCG GCA CGG TTC GCC
Q88HU1_R6_rev	CCG GAA AGG TTT CAT CCA GCG CGT TAT CCA CCG CGC TTT CGC CCG GTT TTT CGC C
Q88HU1_R7_rev	GTT CCC CCC GGG TCA CGG GCT AAT CGG ATC GCT CGC CGG AAA GGT TTC ATC CAG
Q88HU1_sh_R5_rev	GTT CCC CCC GGG TCA TTT TTC GCC GCA ATG GCA ATC CTG CAT GCG GCA CGG TTC GCC
Q88HU1_C28S_fwd	CAA AGC GTA TTG CAG CGA AGC GTG CG
Q88HU1_C28S_rev	CGC ACG CTT CGC TGC AAT ACG CTT TG
J2EKT7_S29C_fwd	GAA GCC TAT TGC TGC CAG GCC TGT G
J2EKT7_S29C_rev	CAC AGG CCT GGC AGC AAT AGG CTT C

Table S2. Chemical shifts and integrals of ^{113}Cd peaks in the 1D spectra depicted in Figures 5 and 6 of the main text.

Cd_4sh_PflQ2 MT		Cd_4S29Csh_PflQ2 MT		Cd_3sh_PflQ2 MT		Cd_3S29Csh_PflQ2 MT	
δ/ppm	Integrals	δ/ppm	Integrals	δ/ppm	Integrals	δ/ppm	Integrals
713.8	1.00	708.7	1.00	695.3	1.00	689.9	0.83
615.4	0.78	619.3	0.90	675.6	0.86	674.9	0.87
585.8	0.93	585.5	0.97	561.6	0.7	569.4	1.00
535	(0.35)*	549.2	0.81				

* This value is only visible at high temperature (320 K).

Table S3. Metal-ligand connectivities of the Cd_4 cluster in S29C-sh_PflQ2 MT. Connectivities obtained from [^{113}Cd, ^{1}H]-HSQC-TOCSY spectra are marked in black, those resulting from structure calculations in red. For the involvement of H36 in coordination see the main text.

Cd (708.7 ppm)	Cd (619.3 ppm)	Cd (585.5 ppm)	Cd (549.2 ppm)
C5	**C10**	**C10**	**(H36)**
C10	**C42**	**C12**	**C7**
C28	**C47**	**C29**	**C32**
C32	**C49**	**C42**	**C49**

Table S4. Details of the structure calculation of Cd_4S29C-sh_PflQ2 MT.

	Cd_4S29C-sh_PflQ2 MT
Input data for structure calculation	
NOE distance restraints	
total	1138
short-range, i-j<2	912
medium range, 1>i-j>5	79
long-range, i-j ≥5	147
Structure statistics, 20 conformers	
CYANA target function value ($Å^2$)	0.52-0.59 (average: 0.56)
Ramachandran plot analysis (Procheck)	residues: all
Residues in favoured regions (%)	68.4
Residues in additional allowed regions (%)	31.6
Residues in generously allowed regions (%)	0
Residues in disallowed regions (%)	0

References:

1 J. Habjanič, O. Zerbe and E. Freisinger, *Metallomics*, 2018, **10**, 1415–1429.